

Unusual water hydrogen bond network around hydrogenated nanodiamonds

Tristan Petit, Ljiljana Puskar, Tatiana Dolenko, Sneha Choudhury, Eglof Ritter, Sergey Burikov, Kirill Laptinskiy, Quentin Brzustowski, Ulrich Schade, Hayato Yuzawa, et al.

▶ **To cite this version:**

Tristan Petit, Ljiljana Puskar, Tatiana Dolenko, Sneha Choudhury, Eglof Ritter, et al.. Unusual water hydrogen bond network around hydrogenated nanodiamonds. Journal of Physical Chemistry C, 2017, 121 (9), pp.5185 - 5194. 10.1021/acs.jpcc.7b00721 . cea-01791642

HAL Id: cea-01791642
https://cea.hal.science/cea-01791642

Submitted on 17 Apr 2023

HAL is a multi-disciplinary open access archive for the deposit and dissemination of scientific research documents, whether they are published or not. The documents may come from teaching and research institutions in France or abroad, or from public or private research centers.

L'archive ouverte pluridisciplinaire **HAL**, est destinée au dépôt et à la diffusion de documents scientifiques de niveau recherche, publiés ou non, émanant des établissements d'enseignement et de recherche français ou étrangers, des laboratoires publics ou privés.



Distributed under a Creative Commons Attribution 4.0 International License

This is an open access article published under an ACS AuthorChoice License, which permits copying and redistribution of the article or any adaptations for non-commercial purposes.

THE JOURNAL OF PHYSICAL CHEMISTRY C

Article

pubs.acs.org/JPCC

Unusual Water Hydrogen Bond Network around Hydrogenated Nanodiamonds

Tristan Petit,*[,†] Ljiljana Puskar,[†] Tatiana Dolenko,[‡,§] Sneha Choudhury,[†,∥] Eglof Ritter,[⊥] Sergey Burikov,[‡] Kirill Laptinskiy,[‡] Quentin Brzustowski,[†] Ulrich Schade,[†] Hayato Yuzawa,[#] Masanari Nagasaka,[#] Nobuhiro Kosugi,[#] Magdalena Kurzyp,[▽] Amélie Venerosy,[▽] Hugues Girard,[▽] Jean-Charles Arnault,[▽] Eiji Osawa,[○] Nicholas Nunn,[◆] Olga Shenderova,[◆] and Emad F. Aziz[†,∥,#,¶]

[†]Methods for Material Development, Helmholtz-Zentrum Berlin für Materialien und Energie GmbH, Albert-Einstein-Strasse 15, 12489 Berlin, Germany

[‡]Physical Department, Moscow State University, 119991 Moscow, Russia

[§]National Research Nuclear University MEPhI, 115409, Kashirskoe Avenue 31, Moscow, Russia

[∥]Department of Physics, Freie Universität Berlin, Arnimallee 14, 14195 Berlin, Germany

[⊥]Experimentelle Biophysik, Institut für Biologie, Humboldt-Universität zu Berlin, 10099 Berlin, Germany

[#]Institute for Molecular Science, Myodaiji, Okazaki 444-8585, Japan

[▽]Diamond Sensors Laboratory, CEA, LIST, F-91191 Gif-sur-Yvette, France

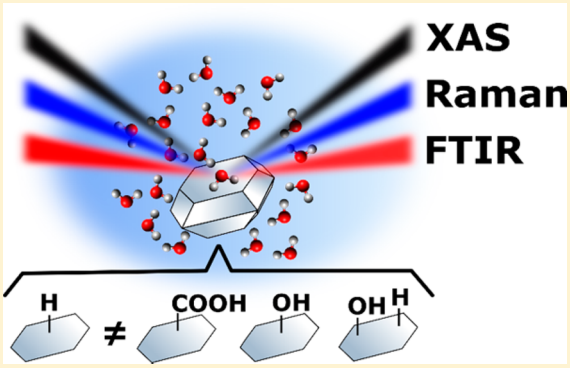
[○]Nanocarbon Research Institute, Shinshu University, Ueda, Nagano 386-8567, Japan

[◆]Adámas Nanotechnologies, Inc., 8100 Brownleigh Drive, Suite 120, Raleigh, North Carolina 27617, United States

[¶]School of Chemistry, Monash University, Clayton, Victoria 3800, Australia

Supporting Information

ABSTRACT: Nanodiamonds exhibit exceptional colloidal properties in aqueous media that lead to a wide range of applications in nanomedicine and other fields. Nevertheless, the role of surface chemistry on the hydration of nanodiamonds remains poorly understood. Here, we probed the water hydrogen bond network in aqueous dispersions of nanodiamonds by infrared, Raman, and X-ray absorption spectroscopies applied in situ in aqueous environment. Aqueous dispersions of nanodiamonds with hydrogenated, carboxylated, hydroxylated, and polyfunctional surface terminations were compared. A different hydrogen bond network was found in hydrogenated nanodiamonds dispersions compared to dispersions of nanodiamonds with other surface terminations. Although no hydrogen bonds are formed between water and hydrogenated surface groups, a long-range disruption of the water hydrogen bond network is evidenced in hydrogenated nanodiamonds dispersion. We propose that this unusual hydration structure results from electron accumulation at the diamond−water interface.



INTRODUCTION

The nanoparticle−water interface plays a central role in nanoparticle reactivity in aqueous environments.[1] The organization of water molecules around dispersed nanoparticles is believed to affect the colloidal stability,[2] the interaction with cellular environment,[3] the chemical and catalytic reactivity,[4] or the optical properties[5] of the nanoparticles. Nanoparticles can also modify solvent properties, leading to more efficient lubricants[6] or thermal fluids[7] for example.

The diamond−water interface is a key model system for interfacial phenomena in water because it is possible to tune the diamond hydrophilicity by modifying its surface chemistry.[8] Oxidized and hydrogenated diamond bulk surfaces are often used as reference for hydrophilic and hydrophobic surfaces, respectively.[9−11] In addition, the negative electron affinity of hydrogenated diamond makes this material unique to investigate charge transfer[10,12] and charge accumulation[11,13,14] phenomena in aqueous media.

At the nanoscale, the hydration structure of hydrogenated nanodiamonds (NDs) remains unknown. Detonation hydrogenated NDs with sizes around 3−5 nm have demonstrated good colloidal stability in water with highly positive ζ-potential in water up to pH 12.[15,16] This behavior seems different from

Received: January 23, 2017
Published: February 15, 2017

Downloaded via CEA SACLAY on April 17, 2023 at 14:39:16 (UTC).
See https://pubs.acs.org/sharingguidelines for options on how to legitimately share published articles.

© 2017 American Chemical Society

DOI: 10.1021/acs.jpcc.7b00721
J. Phys. Chem. C 2017, 121, 5185−5194

hydrogenated bulk diamond, which have negative ζ-potential at neutral or basic pH.[10,14] Furthermore, other hydrophobic carbon nanoparticles such as fullerenes[17] or carbon nanotubes[18] usually present negative ζ-potential in water, therefore a different hydration structure than classical hydrophobic nanoparticles is expected. Early results on hydration of detonation NDs have already been reported,[19,20] however the role of surface chemistry on the hydration structure remains unclear. A previous Raman spectroscopy study focusing on water OH stretching vibrations has demonstrated surface-dependent hydrogen bonding between NDs and water molecules in the first hydration shell, but hydrogenated surfaces were not considered.[5] Stehlik et al. have also demonstrated different hydration behavior between oxidized and hydrogenated detonation NDs by Fourier transformed infrared (FTIR) spectroscopy and further studies are required to have a clear understanding of the diamond−water interface.[21]

In this work, we probed the hydrogen bond (HB) network of water molecules within aqueous dispersions of NDs of different surface chemistries using FTIR, Raman, and X-ray Absorption (XA) spectroscopies. Aqueous dispersions from detonation NDs with hydrogenated (NDs-H), carboxylated (NDs-COOH), hydroxylated (NDs-OH), and polyfunctional (NDs-poly) surfaces were compared. Carboxylated NDs produced by high pressure−high temperature (NDs-HPHT) with a mean diameter of ∼15 nm were also considered to allow for estimation of any size related effect of NDs.

FTIR,[22,23] Raman,[24−26] and XA spectroscopies[27−30] have been extensively applied to probe the HB network of aqueous solutions, however only a few reports on NDs dispersions are yet available.[5,20,31] In this study, vibrational states of OH bonds are probed by FTIR and Raman spectroscopy, whereas XA spectroscopy provides further information on the unoccupied electronic states of oxygen atoms in water molecules. Both electronic and vibrational states are affected by hydrogen bonding, therefore a full picture of water HBs modifications induced by NDs is provided by combination of FTIR, Raman, and XA spectroscopies.

MATERIALS AND METHODS

Nanodiamonds Preparation. Carboxylated and hydroxylated detonation NDs as well as HPHT NDs were provided by Adamas Nanotechnologies, Inc. Detonation NDs were thermally oxidized in air at elevated temperature and then subsequently fractioned to 5 nm primary particles, yielding ND-COOH. NDs-HPHT have followed the same oxidation process. To produce NDs-OH, NDs-COOH were then treated with lithium aluminum hydride (LAH) at elevated temperature under reflux. The reaction mixture was subsequently quenched with 6 M HCl until hydrogen gas evolution ceased, and NDs were washed consecutively with deionized water until a neutral pH was obtained. The measured ζ-potential shift from approximately −35 to +35 mV indicated the reaction had proceeded successfully. The ND-OH material was subsequently fractioned to approximately 30 nm aggregate sizes.

Hydrogenation of NDs was performed using a mass of 40 mg of carboxylated detonation NDs deposited in a quartz tube and inserted in a plasma Downstream source (Sairem SAS, France). High-purity hydrogen gas (>N70) was used with a flow of 10 sccm to maintain a pressure of 12.5 mbar during the treatment. Plasma was generated in the quartz tube at a microwave power of 250 W (2.45 GHz) and the temperature of the NDs during treatment was estimated to be 800−850 °C. During the plasma, the tube is air-cooled. NDs were exposed to hydrogen plasma for 20 min and cooled down under hydrogen for 10 min, leading to ND-H. ND-H were then dispersed in ultrapure water by sonication (UP400S, 400W, 24 kHz, Hielscher Ultrasonics GmbH, Germany) for 1 h under cooling. Larger aggregates were removed from the solution by centrifugation at 4000 rpm (30 min).

NDs-poly dispersion was produced by the Nanocarbon Research Institute by bead-assisted milling as described previously.[32] NDs-poly correspond to nanoAmando samples synthesized in 2015 and have a diameter of ∼3 nm.[33]

All the NDs were dispersed in pure deionized water. Size and ζ-potential measurements were performed on a Zetasizer Nano ZS (Malvern Instruments Ltd. UK) and are summarized in Supporting Information (SI).

Fourier Transformed Infrared Spectroscopy. FTIR measurements were performed using a Bruker Vertex 80v spectrometer with a liquid nitrogen-cooled MCT detector. The spectral resolution was set to 4 cm^{-1}. The spectra were recorded in attenuated total reflectance (ATR) single-reflection mode using a ZnSe crystal. The in-house built environmental cell consists of a small chamber above the ATR crystal (volume of ∼2 mL) with an inlet and outlet allowing the exposure of the sample to gas or liquid. The sample chamber and the whole infrared path were kept under vacuum during the measurements and only the environmental cell chamber was exposed to dry air, humid air, or liquid water. After liquid exposure, some NDs might have been desorbed from the ATR crystal.

For each sample, a reference spectrum was acquired from a clean ATR crystal after 1 h of flushing with dry air to remove any atmospheric contribution (1024 scans were used). A drop of NDs dispersion (100 μL, ∼0.7 mg/mL) was then drop-casted on the crystal and dried overnight. Dry sample spectra were recorded under a flow of dry air. Humid air was prepared by bubbling dry air in a bubbler filled with deionized water (relative humidity of ∼60−70%). All NDs spectra were recorded with an average of 128 scans.

After each sample, the ZnSe crystal was cleaned by ethanol, acetone, and water and new reference spectra were measured to validate the removal of all NDs sample.

Raman Spectroscopy. Raman measurements were performed using excitation by argon laser with wavelength 488 nm and power 350 mW. For suppression, elastic scattering edge-filter Semrock was used. System of registration consisted of monochromator (Acton 2500i, focal length 500 mm, grade 900 grooves/mm) and CCD-camera (Horiba Jobin Yvon, Synapse 1024*128 BIUV, width of entrance slit 25 μm, resolution 2 cm^{-1}). Registration of spectra was performed in one spectral range with center at 580 nm (Raman OH stretching band). Processing of spectra consisted of subtraction of fluorescence background (minimal value), smoothing by Fourier method, correction by transmission spectrum in the given spectral range and normalization on total area of the stretching band. Thermo-stabilizing system allowed setting up and controlling the temperature of the sample with accuracy 0.1 °C.

X-ray Absorption Spectroscopy. The experiments were performed using the soft X-ray undulator beamline BL3U at UVSOR-III Synchrotron with a transmission liquid cell previously described.[34] The NDs dispersion sample was sandwiched between two 100 nm thick Si_3N_4 membranes (NTT AT Co., Ltd.) with pressed Teflon spacers set between the window frames of the membranes and can be substituted by other samples in combination with a tubing pump system. The

DOI: 10.1021/acs.jpcc.7b00721
J. Phys. Chem. C 2017, 121, 5185−5194

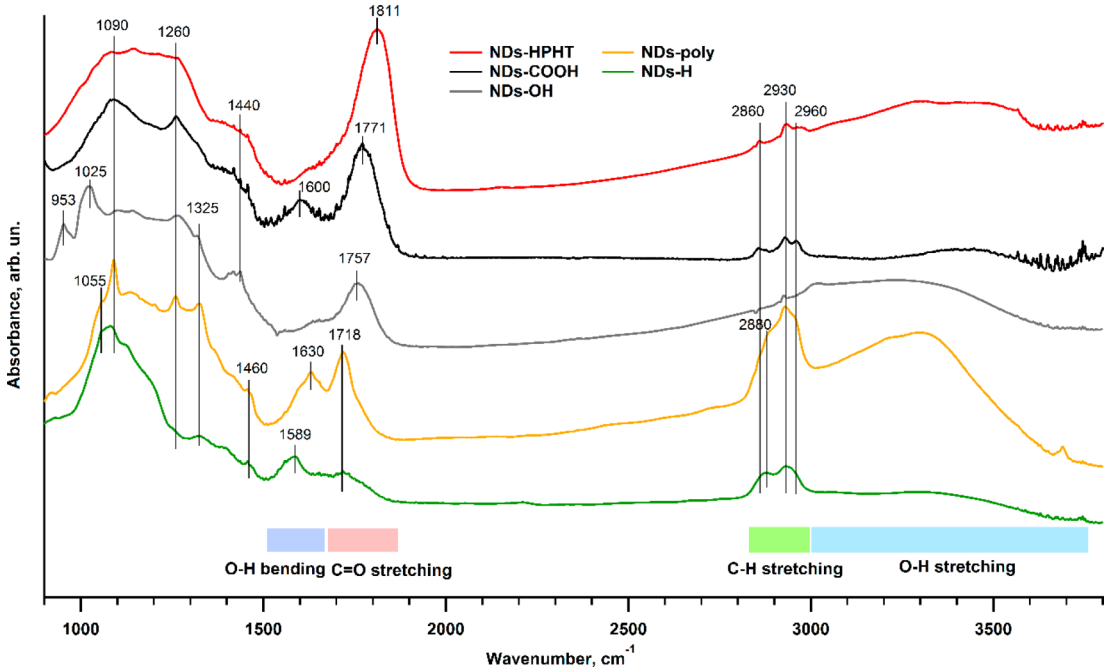


Figure 1. FTIR comparison of NDs having different surface chemistry under dry air flow. The main features impacted by water dispersion are highlighted below the FTIR spectra. The spectra were shifted and normalized for clarity.

thickness of liquid layer was optimized in order to transmit soft X-rays with an appropriate absorbance. The energy resolutions of incident soft X-rays at the O K edge is 0.40 eV. The XA spectra are based on the Beer−Lambert law, $\ln(I_0/I)$, where I_0 and I are the detection current through the cell without and with samples, respectively. The liquid flow is stopped during the XA measurement because the samples are not sensitive to radiation damage under our experimental conditions. The photon energy in the O K edge is calibrated by the O 1s π^* peak (530.80 eV) for free O_2 molecules mixed with helium gas.

RESULTS AND DISCUSSION

Surface Chemistry of Dry Nanodiamonds. The characterization of the surface chemistry of NDs was done by FTIR spectroscopy in ATR mode using an environmental cell. The measurements were performed under dry air flow at room temperature following overnight drying thus ensuring that most of the bulk water is removed without modifying the surface chemistry of NDs (Figure 1). A few water molecules may remain on the NDs surface since the samples were not annealed.

The broad absorbance in the region 900−1500 cm^{-1} present in all spectra of investigated NDs comes from vibrations of the diamond core and the surface chemistry of NDs. On NDs-OH, the features at 953 and 1025 cm^{-1} could be related to C—O vibration from oxidized surface groups.[35] The large band at around 1000−1200 cm^{-1} observed on all NDs has been attributed to overlapping features from defects in the diamond core, ether-like bonds, or hydroxyl groups.[36−40] The feature at 1090 cm^{-1}, particularly sharp on NDs-poly, could be related to C—O stretching in groups such as CH_2OH.[41] The peak at 1260 cm^{-1}, is most likely related to ether-like structure[38,39] at the surface of the NDs, which are removed after hydrogenation treatment. The 1325 cm^{-1} band, observed on NDs-OH, NDs-poly, and NDs-H has previously been attributed to C—H vibrations, coupled to nitrogen-defect in diamond.[38] The small peaks around 1440 cm^{-1} observed on oxidized NDs result from OH bending modes from carboxylic groups.[40] C_{sp3}-H bending modes are detected at 1460 cm^{-1} on NDs-poly and NDs-H.[37]

A broad band is observed at around 1589 cm^{-1} for NDs-H sample. A similar feature reported for hydrogenated NDs[16,21,31] was associated with C═C vibrations from aromatic surface reconstructions. However, the presence of organized aromatic shells stable in air remains controversial and has not yet been reported on detonation NDs.[42−44] No clear sp^2 carbon contribution was detected at the carbon C 1s by X-ray photoelectron spectroscopy on our samples (see SI). Even on surface-graphitized NDs, the sp^2 carbon signature disappears after dispersion in water.[45,46] Finally, C═C modes detected by Raman spectroscopy in the range 1560−1600 cm^{-1} on sp^2-hybridized carbon materials such as fullerenes and nanotubes have shown not to be IR active in previous studies.[47,48] We therefore rather attribute this peak to OH bending from water molecules adsorbed on NDs-H as discussed later.

Strong bands observed at 1757, 1771, and 1811 cm^{-1} for NDs-OH, NDs-COOH, and NDs-HPHT, respectively, are most likely associated with C═O bonds. These C═O bonds are mainly caused by carboxylic groups vibrations in NDs-COOH and NDs-HPHT and carbonyl groups resulting from incomplete chemical reduction of NDs-OH.[37,38,49] The higher frequency observed for the NDs-HPHT could be due to anhydride groups or to the larger size of the NDs crystals.[37] A sharper band observed at 1718 cm^{-1} in NDs-poly is also most likely related to carbonyl or lactone groups.[33,50,51] This feature appears as a weak band for NDs-H.

Absorbance bands found in the spectra of all NDs in the region of 2830−2980 cm^{-1} are related to CH stretching vibrations.[52] For the NDs-H and NDs-poly, broad features around 2880 and 2930 cm^{-1} related to symmetric and asymmetric CH stretching vibrations, respectively, are typical of hydrogen-terminated groups on detonation NDs.[38] These bands are broadened by different contributions from CH, CH_2, and CH_3 groups as discussed in SI. On NDs-COOH and NDs-

DOI: 10.1021/acs.jpcc.7b00721
J. Phys. Chem. C 2017, 121, 5185−5194

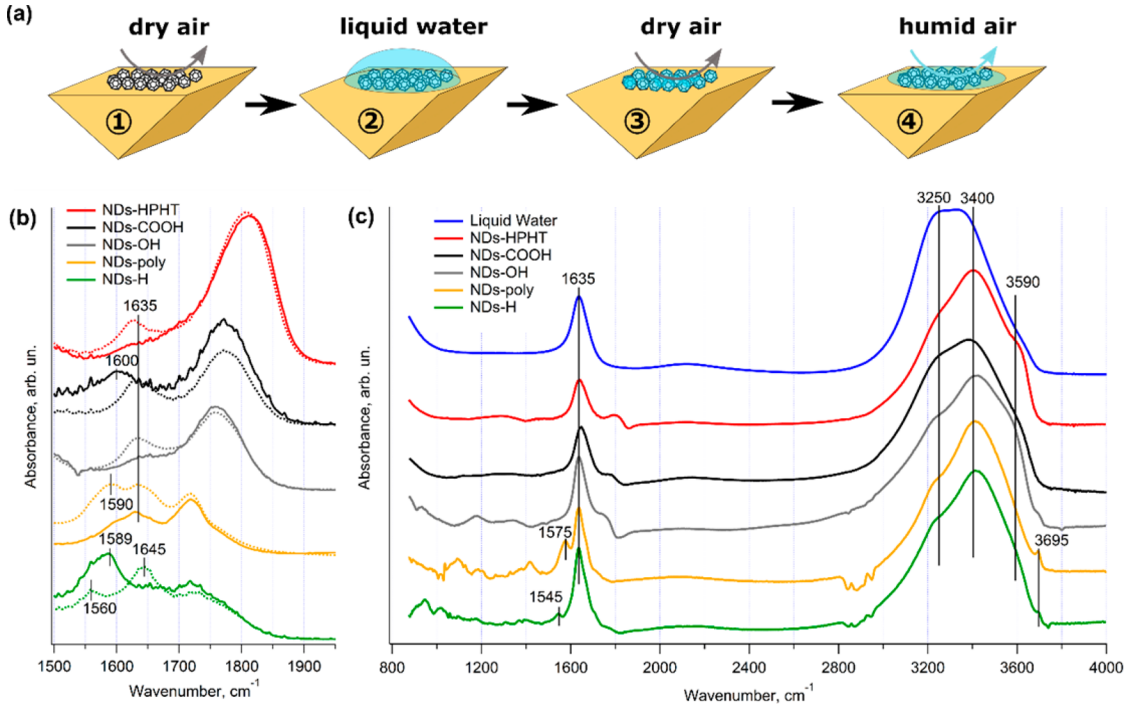


Figure 2. (a) Sequence of FTIR measurements of NDs in the ATR environmental cell. Step 1: NDs are dried overnight and measured under dry air flow. Step 2: NDs are exposed to liquid water. Step 3: NDs are exposed to dry air for a few minutes. Step 4: NDs are exposed to humid air. (b) Comparison of FTIR spectra in the OH bending vibration region between NDs at step 1 (solid) and step 3 (dashed). (c) FTIR difference spectra between steps 4 and 3. The spectrum of liquid water (blue) is shown for comparison. The spectra were normalized for clarity.

HPHT, a different signature consisting of three distinctive peaks at 2960, 2930, and 2860 cm^{-1} is observed, which might originate from different H-terminated groups, though hydrocarbon contamination cannot be ruled out.[52]

The bands in the 1500−1650 and 3200−3600 cm^{-1} regions are associated with OH bending and stretching modes, respectively. Carboxyl groups on NDs-HPHT and NDs-COOH[31,37] as well as hydroxyl groups on NDs-OH[49,53] and NDs-poly[32] are certainly contributing to these bands, but they cannot be reliably distinguished from strongly adsorbed water molecules at room temperature. These bands will therefore be discussed in the following section.

FTIR Characterization of Water Adsorption on Nanodiamonds. The water adsorption on dry NDs surface was characterized by sequentially exposing the NDs in the ATR environmental cell to liquid water and humid air (Figure 2a). The dry NDs (step 1) were exposed to liquid water for a few minutes (step 2). However, the strong OH vibrations bands of bulk water screen the contribution of the first hydration shells interacting with the NDs and no significant difference between liquid water on NDs and pure water was observed (see SI). Dry air was flown over the NDs surface for a few minutes until most of the contribution from bulk water is not detected anymore (step 3). The OH bending regions of the resulting NDs having a thin interfacial water layer are compared to NDs dried overnight in Figure 2b.

The frequency of the OH bending vibration of water molecules shifts depending on the water hydrogen bonding.[23,54,55] The OH bending mode of water monomer in the vapor phase and not bonded to any other water molecules was reported at 1589 cm^{-1}.[23,56] Prior to liquid water exposure, a peak appears around this frequency on NDs-H and a shoulder at 1590 cm^{-1} is also visible on NDs-poly. Non-hydrogen-bonded water molecules are therefore observed on NDs-poly and NDs-H after overnight drying, which could be related to the presence of water molecules on hydrophobic groups, most probably associated with hydrogenated surface groups. The OH bending mode shifts to higher frequencies when HBs are formed.[23,55] A broad band at 1600 cm^{-1} is observed on NDs-COOH while a small shoulder is detected at 1635 cm^{-1} on NDs-HPHT and NDs-OH.

After partial drying of the samples exposed to liquid water (step 3), the OH bending mode appears at 1635 cm^{-1} for all the NDs expect NDs-H (Figure 2b). On NDs-poly, the component at 1590 cm^{-1} is strengthened. On NDs-H, two peaks at 1560 and 1645 cm^{-1} are measured. The OH bending vibrations can vary in the range 1600−1650 cm^{-1} for small water clusters having different HB networks[55,57] and is detected at 1635 cm^{-1} for liquid water (Figure 2c). The variations of OH bending vibration in this range might be related to different water cluster configurations remaining on the partially dried NDs surface and it is therefore difficult to assign all the vibration shifts to surface-dependent HB networks. The feature around 1590 cm^{-1} can however safely be assigned to non-hydrogen-bonded water.

It was found that exposure of the NDs to humid air (step 4) induces a more progressive increase of the water OH vibrational bands with humid air compared to liquid water and can be followed by FTIR. Figure 2c shows the difference spectra, obtained by subtracting the spectra of NDs exposed to humid air for approximately 60 s (step 4) from the dry NDs (step 3). These difference spectra have the advantage of only presenting the IR contribution arising from adsorbed water molecules and the related changes of NDs surface chemistry.

In the OH bending mode region, a significant increase of the liquid water component at 1635 cm^{-1} demonstrates strong

DOI: 10.1021/acs.jpcc.7b00721
J. Phys. Chem. C 2017, 121, 5185−5194

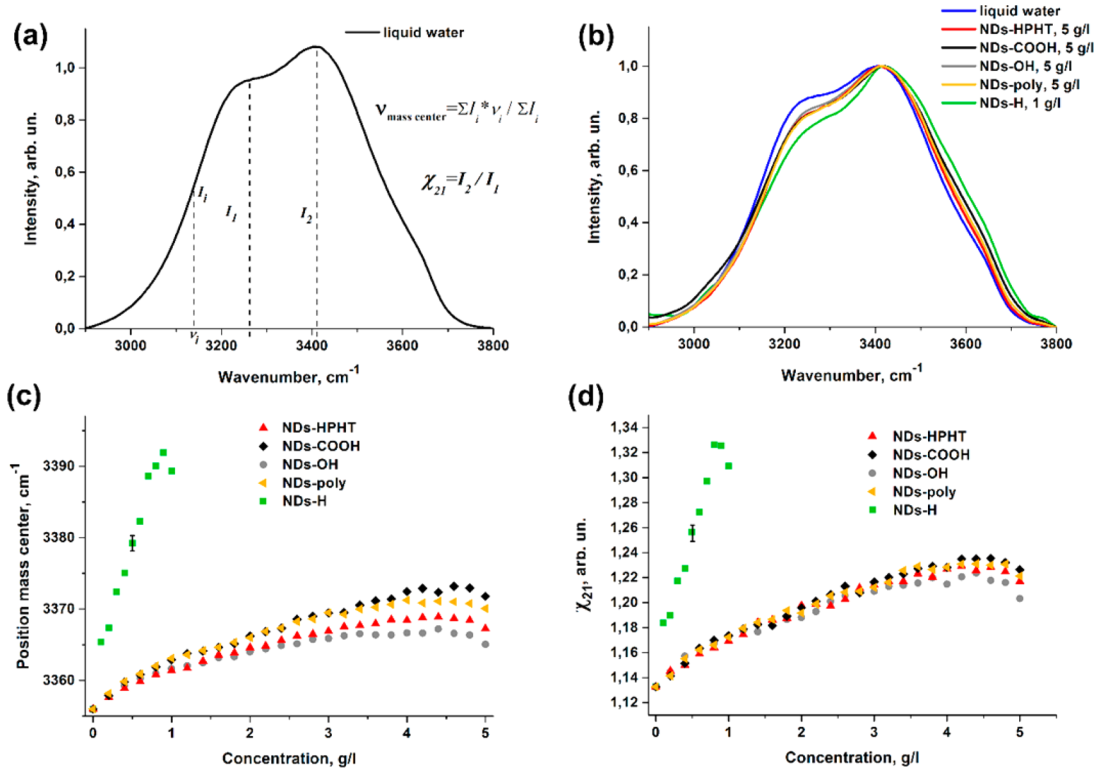


Figure 3. (a) Illustration of calculation of the position of mass center (ν_{mc}) and parameter χ_{21} of water Raman OH stretching bands. (b) Raman OH stretching bands of aqueous dispersions of NDs. The spectra were normalized to the maximum I_2 of the stretching bands. Dependence of ν_{mc} (c) and χ_{21} (d) in NDs aqueous dispersions with respect to the NDs concentration.

adsorption of water molecules on the NDs. A clear separate peak appears at 1545 and 1575 cm^{-1} for NDs-H and NDs-poly, respectively. The shift to lower frequencies than reported for water monomer (1589 cm^{-1}) is quite surprising because HB formation should shift the OH bending mode toward higher frequencies. This behavior was reproduced on NDs-H prepared from a different detonation material (see SI).

In the 1800 cm^{-1} region, a dip followed by a broad peak at lower frequency is observed for NDs-HPHT, NDs-COOH, and NDs-OH, caused by an ~6−7 cm^{-1} shift of the C═O bonds peak to lower frequency. The shift is probably induced by electrostatic interaction between C═O and hydrogen from water molecules resulting from the formation of HBs.[37,58]

The absorbance bands in the region of 2800−3000 cm^{-1} due to the CH stretching bands decrease on NDs-H and NDs-poly with exposure to humid air, as evidenced by the negative contribution in the difference spectra. No changes are observed for oxidized NDs. Frequency shift and change in absorbance of the CH stretching bands can provide information on the chemical environment of the CH bonds[59] and the formation of HBs.[54,60,61] A careful investigation of the changes induced in the CH stretching region by water adsorption reveals that the frequency of the different CH stretching components remains more or less constant with water exposure (see SI). This result would suggest that no HBs are formed between water molecules and CH_x groups. However, the relative IR absorbance increase could be related to polarization of the CH_x groups,[59] which might be affected by water adsorption.

Finally, water adsorption also promotes the increase of OH stretching modes in the region 3000−3600 cm^{-1} which are highly sensitive to water HB network.[22,62] The broad band consists of three main components peaking at 3250, 3400, and 3590 cm^{-1}. The bands at 3250 and 3400 cm^{-1} are usually related to water molecules in tetrahedral-bonded ice-like organization and in HB-distorted liquid environment, respectively.[22,62,63] The band at 3590 cm^{-1} corresponds to poorly connected water molecules as observed in water clusters.[22] The relative absorbance of the OH stretching bands is often considered in order to estimate the overall water organization changes.[62−64] On NDs, the decrease of the bands at 3250 cm^{-1} compared to liquid water demonstrates a lower coordination of water molecules than in pure liquid water. The absorbance of the OH stretching bands depends though significantly on the water coverage of the NDs, which might vary for the different surface-terminated NDs in the ATR environmental cell. As a result, the surface-dependent relative changes of the OH stretching bands will rather be analyzed from Raman measurements recorded in liquid dispersions at known concentrations in the next section.

A small peak at 3695 cm^{-1}, observed for NDs-H and NDs-poly and already present in the dry NDs spectra, is associated with vibrations of free- or non-hydrogen-bonded OH groups.[21] This feature has previously been reported for water molecules adsorbed on hydrophobic surfaces.[65]

Influence of Nanodiamonds Dispersion on Water Raman OH Stretching Bands. While the OH stretching bands for NDs in liquid water (step 2) looked similar in FTIR spectra (see SI), significant differences between the various NDs samples were observed in aqueous dispersions by Raman spectroscopy as shown in Figure 3.

The high-frequency component of the stretching band (with a maximum I_2) is caused by vibrations of the OH groups with weak HBs, and the low-frequency component (with a maximum I_1), by vibrations of OH groups with strong

DOI: 10.1021/acs.jpcc.7b00721
J. Phys. Chem. C 2017, 121, 5185−5194

HBs.[66−68] These features are similar to the OH stretching bands in the 3000−3800 cm^{-1} region previously discussed in FTIR characterization. The parameter χ_{21}, defined as the ratio I_2/I_1 (see Figure 3a), characterizes the share of weakly bonded OH groups in the solution in relation to the strongly bonded OH groups. An increase of the χ_{21} value therefore indicates a weakening of HBs in the NDs dispersion. Analogously, one can explain a change in position of the mass center of the band (ν_{mc}, Figure 3a). When HBs are weakened, the frequency of stretching vibrations of hydrogen groups increases, shifting the mass center toward high frequencies.

The evolution of parameters ν_{mc} and χ_{21} for all NDs dispersions at various concentrations is plotted in Figure 3, panels c and d, respectively. From the results, one can see that for all NDs studied, values of the two parameters, namely the position of mass center and the ratio χ_{21} of water Raman OH stretching band, are both larger in comparison to pure water. These parameters increase with the NDs concentration until a critical value (around 0.9 mg/mL for NDs-H and 4.5 mg/mL for other NDs) is reached. Above this critical concentration, the decrease of these parameters might result from NDs aggregation, reducing the surface area that is exposed to solvent molecules. However, within the range of NDs concentration used, values of these parameters are found to increase to different extents depending on the ND surface chemistry. From the dependencies of ν_{mc} and χ_{21} on the NDs concentration, the following ordering, going from the highest to lowest HBs weakener, can be obtained

$$\text{NDs-H} > > \text{NDs-COOH} \geq \text{NDs-poly} > \text{NDs-HPHT} > \text{NDs-OH}$$

The difference between NDs-COOH and NDs-OH was reported to be due to a weaker HB strength between C═O groups and water molecules as compared to hydroxylated surfaces.[5] The difference between NDs-COOH and NDs-HPHT could be attributed to a larger surface area of the detonation NDs-COOH, inducing higher distortion of the water structure.

The impact of NDs-H on water HB network is much more significant than for the other NDs. Compared to other NDs termination, similar modification of the OH stretching bands for NDs-H occurs at 1 order of magnitude lower concentration. Above a concentration of 0.5 g/L, the shift toward higher frequencies of the Raman water OH stretching band in the NDs-H dispersion is larger than in other dispersions at 5 g/L. This means that the HB network around NDs-H is much weaker than HBs formed in pure water or between water molecules and the surface groups of the other NDs. This is also seen by the relative increase of the component at 3600 cm^{-1}, associated with water molecules coordinated in a weak HB network (Figure 3b). This behavior is as expected from the hydrophobic nature of the H-terminated diamond surface. The difference to pure water cannot be explained solely by the water molecules in the first hydration shells of the NDs-H surface. It is more likely that NDs-H perturb the water HB network over several tens of nanometers, which differs from other NDs dispersions at the same concentration and size.

It is somewhat surprising that NDs-poly do not behave more similarly to NDs-H, considering their FTIR signatures were close. On the NDs-poly surface, hydroxyl groups are also present and are able to form strong HBs with water molecules. The HB network is nevertheless weakened when compared to purely hydroxylated NDs due to the CH_x groups behaving as hydrophobic sites that locally disturb the water HB network.

Influence of Nanodiamonds Dispersion on Water Oxygen K Edge X-ray Absorption. XA spectroscopy measured in transmission mode at the oxygen K edge is sensitive to HB network of aqueous solutions.[27−29] Water XA spectra show a pre-edge around 535 eV, a main edge at 538 eV, and a postedge around 540 eV. The first two peaks are usually interpreted as features associated with distorted HBs while the postedge is related to long-range ordered HBs networks such as found in tetrahedral ice.[28,69,70]

The XA spectra recorded for the different NDs dispersions are compared in Figure 4. NDs-COOH, NDs-HPHT, and

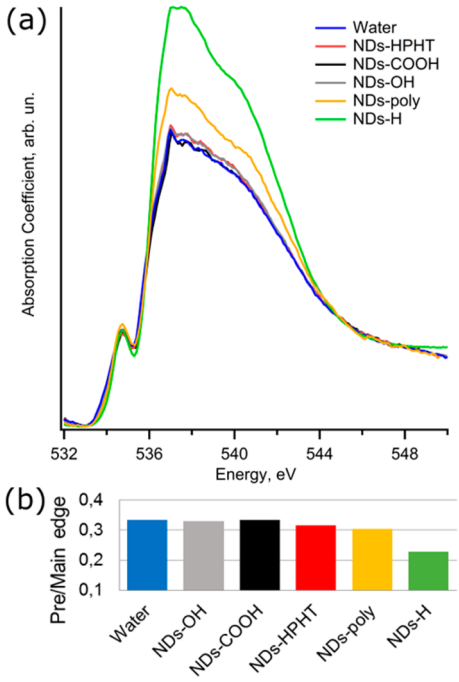


Figure 4. (a) XA spectra of the oxygen K edge of NDs aqueous dispersions at 1 wt % (except NDs-H at 0.5 wt %). The spectra were normalized to before (533 eV) and after (545 eV) the main features. (b) Calculation of pre/main-edge ratio of oxygen K edge XA spectra for NDs dispersions.

NDs-OH have very similar absorption at the main-edge, slightly higher than bulk water. On the other hand, XA spectra of NDs-H and NDs-poly exhibit a prominent increase of the XA in particular at the main- and post-edges. Note that the increase is significantly larger for NDs-H because its concentration is only 0.5 wt % as compared to 1 wt % used for the other NDs in Figure 4a. Surprisingly, the pre-edge feature does not increase as much as the main- and post-edges for NDs-H as deduced from the pre/main-edge ratio plotted in Figure 4b.

The higher absorption at the oxygen K edge, except in the pre-edge region, was proposed to be the signature of a long-range change of water organization around NDs.[20] The increase of the main- and post-edge is indeed extremely large compared to ionic species at higher concentration.[27] These changes cannot only be associated with hydrophobic hydration because previous XA measurements on hydrophobic solutes induced only small changes of the water structure.[29,71,72] The water reorganization around NDs-H thus affects more than the first hydration shell, which is also deduced from Raman results. The

DOI: 10.1021/acs.jpcc.7b00721
J. Phys. Chem. C 2017, 121, 5185−5194

reordered water molecules have most likely both hydrogen involved in HBs, so-called double HB donor (DD) configurations, which was found not to contribute to the pre-edge region.[73] The intensity increase might be due to a higher water density, as evidenced on amorphous ices.[74] The strength of the HBs however remains weak when compared to tetrahedral ice, having an enhanced XA postedge due to delocalization of the unoccupied electronic states over the ice phase.[74,75] The relatively smaller change of XA spectra for NDs-poly is most probably explained by a lower concentration of CH_x groups on their surface, which are therefore associated with the water long-range disruption.

Charge Accumulation at the Hydrogenated Diamond−Water Interface. Distinctive observations from FTIR and XA characterizations were noted for NDs-poly and NDs-H samples, both having surface hydrogenated groups. In particular, OH bending mode is detected at a frequency below the bending vibrational mode reported for water monomer at 1589 cm^{-1} by FTIR.[23,56] This shift to lower energies cannot be related to hydrogen bonding with water molecules as that would shift the frequency of OH bending vibration to the other direction.[23,55] Similar downshift of the OH bending modes was previously reported on water clusters having an excess electron.[76−78] Hammer et al. demonstrated that an extra electron bonded to a water molecule with the two hydrogen not involved in hydrogen bonds, so-called double HB acceptor (AA) configuration, shifts the OH bending mode down to 1540 cm^{-1}.[76] The strong redshift of the bending mode frequency was explained by a charge transfer of the excess electron to the σ^*_{OH} antibonding orbital of the water molecule, stabilizing the extra electron.[77] It is therefore possible that in our case, the peaks at 1560 cm^{-1} after liquid water exposure on NDs-H and at respectively 1545 and 1575 cm^{-1} for NDs-H and NDs-poly after humid air exposure, result from the redshift of OH bending modes induced by charge accumulation at the diamond−water interface. Because of a negative electron affinity, hydrogen-terminated diamond can transfer electrons to neighboring molecules. This phenomenon, called surface transfer doping, has been reported on hydrogen-terminated diamonds[79,80] and NDs.[15] In water, a similar process has been proposed with an oxygen electrochemical redox couple.[10] The hydrophobic character of the H-terminated diamond induces the formation of a hydrophobic gap at the diamond−water interface that enables charge accumulation.[9,11] We expect that accumulation of electrons in the hydrophobic gap at the diamond−water interface would be responsible for the large downshift of the OH bending mode of water molecules around NDs-H. The extra electrons are stabilized by the dangling hydrogen from water molecules that cannot form HBs with the hydrophobic hydrogenated groups. NDs-H prepared in a hydrogen plasma are expected to have a higher surface coverage of CH_x groups than NDs-poly. As a result, the redshift of bending modes is larger for NDs-H than NDs-poly due to a stronger electron accumulation. Competing interactions with hydroxyl groups might also play a role on NDs-poly.

Electrostatic interactions between excess electrons at the water interface and CH_x groups from the diamond surface would be expected. Although no significant frequency shift is observed for the CH stretching region on IR spectra, the relative IR absorbance was proposed as an alternative tool highly sensitive to the charge distribution.[59] In particular, the presence of an excess electron close to the positively charged NDs surface would induce strong polarization of the CH bonds. This polarization is expected to decrease the absorbance of CH stretching bands.[59] In our study, the decrease of the CH stretching band is particularly strong for CH and CH_3 groups, which might be more strongly involved in the stabilization of extra electrons at the diamond-water interface.

Excess electrons at the diamond−water interface would also impact the electronic signature of water molecules in the first hydration shell of NDs-H. The charge transfer of the excess electron to the σ^*_{OH} antibonding orbital of the AA water molecules suggested by IR data would indeed affect the oxygen K edge XA signature.[77] This orbital is expected to contribute to the pre-edge[69] of oxygen K edge water XA spectra, therefore the filling of this orbital would lead to a decrease of the X-ray absorbance in this region. The decrease of the pre-edge observed in Figure 4 is therefore in agreement with the accumulation of excess electrons in the interfacial water layers. Note that water molecules in the first hydration shell of NDs-H would represent only a small contribution of the overall XA spectrum due to the low concentration of NDs-H and the XA spectral changes are mostly resulting from water long-range disruption. The proposed hydration structure around NDs-H in aqueous dispersion is summarized in Figure 5.

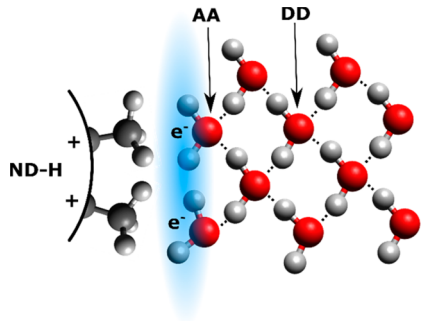


Figure 5. Schematic view of proposed hydrogen bonding between water and positively charged hydrogenated ND surface. Water molecules in double HB acceptor (AA) and donor (DD) configurations are highlighted. The weak HBs are marked with dotted lines.

Positive charges at the NDs-H surface resulting from the charge transfer are most probably responsible of the positive ζ-potential of NDs-H. It should be noted that charge transfer is not the only origin of positive ζ-potential on NDs because NDs-OH also have positive ζ-potential with a very different hydration structure. In this case, the formation of $C—OH_2^+$ in water might be responsible of the positive ζ-potential,[81] although the stability of such group at neutral pH remains questionable. NDs with the same ζ-potential may have very different impact on the water hydrogen bond network and characterization of hydrophilic/hydrophobic sites appears to be a better approach to estimate the hydration structure of NDs.

Hydrophilic and hydrophobic sites can be observed on the same NDs such as NDs-poly due to the presence of hydroxyl and hydrogenated groups. For Raman spectroscopy, the hydrophobic sites on NDs-poly are screened by the hydrophilic ones. On the other hand, XA spectroscopy is more impacted by AA water molecules close to hydrophobic sites due to $e^- \rightarrow \sigma^*_{OH}$ charge transfer. As a result, water interfacial layer on NDs-poly exhibits different XA and Raman signature due to the presence of both hydrophilic and hydrophobic surface sites.

DOI: 10.1021/acs.jpcc.7b00721
J. Phys. Chem. C 2017, 121, 5185−5194

The positive ζ-potential of NDs-poly could originate from both the hydrogenated and the hydroxylated groups.

CONCLUSION

In this work, we characterized the HB network of water molecules in aqueous dispersions of NDs with different surface chemistries using FTIR, Raman, and XA spectroscopies. Water HB network was found to be different in aqueous dispersions of NDs-H compared to dispersions of NDs terminated with other surface groups. CH_x groups do not form HBs with water molecules due to their hydrophobic character. However, a long-range disruption of the water HB network is associated with hydrogenated surface groups, as concluded from Raman and XA spectroscopies, which could be the consequence of an electron accumulation at the hydrogenated diamond−water interface. The excess electrons are likely to be stabilized by water molecules in the first hydration shell of NDs-H, which is evidenced by a shift to lower frequency of the OH bending mode on FTIR and a decrease of the pre-edge of oxygen K edge XA spectra partially due to $e^- \rightarrow \sigma^*_{OH}$ charge transfer. Hydrogenated groups induce a long-range disordering of water molecules around NDs-H and HBs between these water molecules are weaker than those found in bulk water, as observed by the strong change of OH stretching bands in Raman spectra and of the oxygen K edge X-ray absorption of NDs-H dispersions.

The unusual hydration of NDs-H could explain their relatively good colloidal dispersion capability compared to other hydrophobic nanomaterials. Electron accumulation in the NDs-H hydration shell would most probably be related to unique properties of H-terminated diamond in water such as the ability to generate solvated electrons with high reducing ability[82] or to enhance the generation of reactive oxygen species in radioresistant cancer cells.[83] The modification of water HB network around NDs-H should be considered for further studies on the catalytic and chemical reactivity of NDs-H in aqueous media.

ASSOCIATED CONTENT

Supporting Information

The Supporting Information is available free of charge on the ACS Publications website at DOI: 10.1021/acs.jpcc.7b00721.

Dynamic light scattering and X-ray photoelectron spectroscopy characterizations, additional details on ATR-FTIR characterization (PDF)

AUTHOR INFORMATION

Corresponding Author

*E-mail: tristan.petit@helmholtz-berlin.de.

Notes

The authors declare no competing financial interest.

ACKNOWLEDGMENTS

T.P. acknowledges the Volkswagen Foundation (Freigeist Fellowship No. 89592) for financial support. H.Y. is a Research Fellow of the Japan Society of Division for the Promotion of Science. This work was partly supported by European Union's Horizon 2020 research and innovation programme under Grant Agreement 665085, by JSPS Grants-in-Aid for Scientific Research (No. 26248010), by the grants of the Russian Foundation for Basic Research No. 15-29-01290 ofi_m and No. 16-32-00882_mol_a. This work was done in accordance with the Competitiveness Program of NRNU MEPhI. We acknowledge the kind support by staff members of the UVSOR-III Synchrotron Facility.

REFERENCES

(1) Björneholm, O.; Hansen, M. H.; Hodgson, A.; Liu, L.-M.; Limmer, D. T.; Michaelides, A.; Pedevilla, P.; Rossmeisl, J.; Shen, H.; Tocci, G.; et al. Water at Interfaces. *Chem. Rev.* **2016**, *116*, 7698−7726.

(2) Anand, U.; Lu, J.; Loh, D.; Aabdin, Z.; Mirsaidov, U. Hydration Layer-Mediated Pairwise Interaction of Nanoparticles. *Nano Lett.* **2016**, *16*, 786−790.

(3) Nel, A. E.; Mädler, L.; Velegol, D.; Xia, T.; Hoek, E. M. V; Somasundaran, P.; Klaessig, F.; Castranova, V.; Thompson, M. Understanding Biophysicochemical Interactions at the Nano-Bio Interface. *Nat. Mater.* **2009**, *8*, 543−557.

(4) Rubasinghege, G.; Grassian, V. H. Role(s) of Adsorbed Water in the Surface Chemistry of Environmental Interfaces. *Chem. Commun. (Cambridge, U. K.)* **2013**, *49*, 3071−3094.

(5) Dolenko, T. A.; Burikov, S. A.; Rosenholm, J. M.; Shenderova, O. A.; Vlasov, I. I. Diamond−Water Coupling Effects in Raman and Photoluminescence Spectra of Nanodiamond Colloidal Suspensions. *J. Phys. Chem. C* **2012**, *116*, 24314−24319.

(6) Ma, L.; Gaisinskaya-Kipnis, A.; Kampf, N.; Klein, J. Origins of Hydration Lubrication. *Nat. Commun.* **2015**, *6*, 6060.

(7) Xie, H.; Fujii, M.; Zhang, X. Effect of Interfacial Nanolayer on the Effective Thermal Conductivity of Nanoparticle-Fluid Mixture. *Int. J. Heat Mass Transfer* **2005**, *48*, 2926−2932.

(8) Ostrovskaya, L.; Perevertailo, V.; Ralchenko, V.; Dementjev, A.; Loginova, O. Wettability and Surface Energy of Oxidized and Hydrogen Plasma-Treated Diamond Films. *Diamond Relat. Mater.* **2002**, *11*, 845−850.

(9) Bonthuis, D.; Gekle, S.; Netz, R. Dielectric Profile of Interfacial Water and Its Effect on Double-Layer Capacitance. *Phys. Rev. Lett.* **2011**, *107*, 166102.

(10) Chakrapani, V.; Angus, J. C.; Anderson, A. B.; Wolter, S. D.; Stoner, B. R.; Sumanasekera, G. U. Charge Transfer Equilibria between Diamond and an Aqueous Oxygen Electrochemical Redox Couple. *Science* **2007**, *318*, 1424−1430.

(11) Dankerl, M.; Lippert, A.; Birner, S.; Stützel, E.; Stutzmann, M.; Garrido, J. Hydrophobic Interaction and Charge Accumulation at the Diamond-Electrolyte Interface. *Phys. Rev. Lett.* **2011**, *106*, 196103.

(12) Ristein, J. Surface Science of Diamond: Familiar and Amazing. *Surf. Sci.* **2006**, *600*, 3677−3689.

(13) Garrido, J. A.; Härtl, A.; Dankerl, M.; Reitinger, A.; Eickhoff, M.; Helwig, A.; Müller, G.; Stutzmann, M. The Surface Conductivity at the Diamond/aqueous Electrolyte Interface. *J. Am. Chem. Soc.* **2008**, *130*, 4177−4181.

(14) Härtl, A.; Garrido, J. A.; Nowy, S.; Zimmermann, R.; Werner, C.; Horinek, D.; Netz, R.; Stutzmann, M. The Ion Sensitivity of Surface Conductive Single Crystalline Diamond. *J. Am. Chem. Soc.* **2007**, *129*, 1287−1292.

(15) Petit, T.; Girard, H. A.; Trouvé, A.; Batonneau-Gener, I.; Bergonzo, P.; Arnault, J.-C. Surface Transfer Doping Can Mediate Both Colloidal Stability and Self-Assembly of Nanodiamonds. *Nanoscale* **2013**, *5*, 8958−8962.

(16) Williams, O. A.; Hees, J.; Dieker, C.; Jäger, W.; Kirste, L.; Nebel, C. E. Size-Dependent Reactivity of Diamond Nanoparticles. *ACS Nano* **2010**, *4*, 4824−4830.

(17) Ma, X.; Bouchard, D. Formation of Aqueous Suspensions of Fullerenes. *Environ. Sci. Technol.* **2009**, *43*, 330−336.

(18) Jiang, L.; Gao, L.; Sun, J. Production of Aqueous Colloidal Dispersions of Carbon Nanotubes. *J. Colloid Interface Sci.* **2003**, *260*, 89−94.

(19) Korobov, M. V.; Avramenko, N. V.; Bogachev, A. G.; Rozhkova, N. N.; Osawa, E. Nanophase of Water in Nano-Diamond Gel. *J. Phys. Chem. C* **2007**, *111*, 7330−7334.

DOI: 10.1021/acs.jpcc.7b00721
J. Phys. Chem. C 2017, 121, 5185−5194

(20) Petit, T.; Yuzawa, H.; Nagasaka, M.; Yamanoi, R.; Osawa, E.; Kosugi, N.; Aziz, E. F. Probing Interfacial Water on Nanodiamonds in Colloidal Dispersion. *J. Phys. Chem. Lett.* **2015**, *6*, 2909−2912.
(21) Stehlik, S.; Glatzel, T.; Pichot, V.; Pawlak, R.; Meyer, E.; Spitzer, D.; Rezek, B. Water Interaction with Hydrogenated and Oxidized Detonation Nanodiamonds - Microscopic and Spectroscopic Analyses. *Diamond Relat. Mater.* **2016**, *63*, 97−102.
(22) Brubach, J.-B.; Mermet, A.; Filabozzi, A.; Gerschel, A.; Roy, P. Signatures of the Hydrogen Bonding in the Infrared Bands of Water. *J. Chem. Phys.* **2005**, *122*, 184509.
(23) Laporta, M.; Pegoraro, M.; Zanderighi, L. Perfluorosulfonated Membrane (Nafion): FT-IR Study of the State of Water with Increasing Humidity. *Phys. Chem. Chem. Phys.* **1999**, *1*, 4619−4628.
(24) Auer, B.; Kumar, R.; Schmidt, J. R.; Skinner, J. L. Hydrogen Bonding and Raman, IR, and 2D-IR Spectroscopy of Dilute HOD in Liquid D2O. *Proc. Natl. Acad. Sci. U. S. A.* **2007**, *104*, 14215−14220.
(25) Sun, Q. Raman Spectroscopic Study of the Effects of Dissolved NaCl on Water Structure. *Vib. Spectrosc.* **2012**, *62*, 110−114.
(26) Dolenko, T. A.; Burikov, S. A.; Dolenko, S. A.; Efitorov, A. O.; Plastinin, I. V.; Yuzhakov, V. I.; Patsaeva, S. V. Raman Spectroscopy of Water-Ethanol Solutions: The Estimation of Hydrogen Bonding Energy and the Appearance of Clathrate-like Structures in Solutions. *J. Phys. Chem. A* **2015**, *119*, 10806−10815.
(27) Waluyo, I.; Nordlund, D.; Bergmann, U.; Schlesinger, D.; Pettersson, L. G. M.; Nilsson, A. A Different View of Structure-Making and Structure-Breaking in Alkali Halide Aqueous Solutions through X-Ray Absorption Spectroscopy. *J. Chem. Phys.* **2014**, *140*, 244506.
(28) Nilsson, A.; Nordlund, D.; Waluyo, I.; Huang, N.; Ogasawara, H.; Kaya, S.; Bergmann, U.; Näslund, L.-Å.; Öström, H.; Wernet, P.; et al. X-Ray Absorption Spectroscopy and X-Ray Raman Scattering of Water and Ice; an Experimental View. *J. Electron Spectrosc. Relat. Phenom.* **2010**, *177*, 99−129.
(29) Nagasaka, M.; Mochizuki, K.; Leloup, V.; Kosugi, N. Local Structures of Methanol-Water Binary Solutions Studied by Soft X-Ray Absorption Spectroscopy. *J. Phys. Chem. B* **2014**, *118*, 4388−4396.
(30) Lange, K. M.; Aziz, E. F. The Hydrogen Bond of Water from the Perspective of Soft X-Ray Spectroscopy. *Chem. - Asian J.* **2013**, *8*, 318−327.
(31) Ji, S.; Jiang, T.; Xu, K.; Li, S. FTIR Study of the Adsorption of Water on Ultradispersed Diamond Powder Surface. *Appl. Surf. Sci.* **1998**, *133*, 231−238.
(32) Ozawa, M.; Inaguma, M.; Takahashi, M.; Kataoka, F. Krüger, a.; Ōsawa, E. Preparation and Behavior of Brownish, Clear Nanodiamond Colloids. *Adv. Mater.* **2007**, *19*, 1201−1206.
(33) Mchedlov-Petrossyan, N. O.; Kamneva, N. N.; Marynin, a I.; Kryshtal, a P.; Ösawa, E. Colloidal Properties and Behaviors of 3 Nm Primary Particles of Detonation Nanodiamonds in Aqueous Media. *Phys. Chem. Chem. Phys.* **2015**, *17*, 16186−16203.
(34) Nagasaka, M.; Hatsui, T.; Horigome, T.; Hamamura, Y.; Kosugi, N. Development of a Liquid Flow Cell to Measure Soft X-Ray Absorption in Transmission Mode: A Test for Liquid Water. *J. Electron Spectrosc. Relat. Phenom.* **2010**, *177*, 130−134.
(35) Meldrum, B. J.; Rochester, C. H. In Situ Infrared Study of the Surface Oxidation of Activated Carbon in Oxygen and Carbon Dioxide. *J. Chem. Soc., Faraday Trans.* **1990**, *86*, 861.
(36) Mutschke, H.; Dorschner, J.; Henning, T.; Jäger, C.; Ott, U. Facts and Artifacts in Interstellar Diamond Spectra. *Astrophys. J.* **1995**, *454*, L157.
(37) Tu, J.-S.; Perevedentseva, E.; Chung, P.-H.; Cheng, C.-L. Size-Dependent Surface CO Stretching Frequency Investigations on Nanodiamond Particles. *J. Chem. Phys.* **2006**, *125*, 174713.
(38) Jiang, T.; Xu, K. FTIR Study of Ultradispersed Diamond Powder Synthesized by Explosive Detonation. *Carbon* **1995**, *33*, 1663−1671.
(39) Struck, L. M. Interaction of Hydrogen and Water with Diamond (100): Infrared Spectroscopy. *J. Vac. Sci. Technol., A* **1993**, *11*, 1992.
(40) Shin, S.; Jang, J.; Yoon, S.-H.; Mochida, I. A Study on the Effect of Heat Treatment on Functional Groups of Pitch Based Activated Carbon Fiber Using FTIR. *Carbon* **1997**, *35*, 1739−1743.
(41) Ávila-Orta, C. A.; Cruz-Delgado, V. J.; Neira-Velázquez, M. G.; Hernández-Hernández, E.; Méndez-Padilla, M. G.; Medellín-Rodríguez, F. J. Surface Modification of Carbon Nanotubes with Ethylene Glycol Plasma. *Carbon* **2009**, *47*, 1916−1921.
(42) Fang, X.; Mao, J.; Levin, E. M.; Schmidt-Rohr, K. Nonaromatic Core-Shell Structure of Nanodiamond from Solid-State NMR Spectroscopy. *J. Am. Chem. Soc.* **2009**, *131*, 1426−1435.
(43) Petit, T.; Arnault, J.-C.; Girard, H. A.; Sennour, M.; Bergonzo, P. Early Stages of Surface Graphitization on Nanodiamond Probed by X-Ray Photoelectron Spectroscopy. *Phys. Rev. B: Condens. Matter Mater. Phys.* **2011**, *84*, 233407.
(44) Mermoux, M.; Crisci, A.; Petit, T.; Girard, H. A.; Arnault, J.-C. Surface Modifications of Detonation Nanodiamonds Probed by Multiwavelength Raman Spectroscopy. *J. Phys. Chem. C* **2014**, *118*, 23415−23425.
(45) Petit, T.; Arnault, J.-C. C.; Girard, H. A.; Sennour, M.; Kang, T.-Y.; Cheng, C.-L.; Bergonzo, P. Oxygen Hole Doping of Nanodiamond. *Nanoscale* **2012**, *4*, 6792−6799.
(46) Petit, T.; Pflüger, M.; Tolksdorf, D.; Xiao, J.; Aziz, E. F. Valence Holes Observed in Nanodiamonds Dispersed in Water. *Nanoscale* **2015**, *7*, 2987−2991.
(47) Andrievsky, G. V.; Klochkov, V. K.; Bordyuh, A. B.; Dovbeshko, G. I. Comparative Analysis of Two Aqueous-Colloidal Solutions of C60 Fullerene with Help of FTIR Reflectance and UV−Vis Spectroscopy. *Chem. Phys. Lett.* **2002**, *364*, 8−17.
(48) Ellison, M. D.; Good, A. P.; Kinnaman, C. S.; Padgett, N. E. Interaction of Water with Single-Walled Carbon Nanotubes: Reaction and Adsorption. *J. Phys. Chem. B* **2005**, *109*, 10640−10646.
(49) Shenderova, O.; Panich, A. M.; Moseenkov, S.; Hens, S. C.; Kuznetsov, V.; Vieth, H. M. Hydroxylated Detonation Nanodiamond: FTIR, XPS, and NMR Studies. *J. Phys. Chem. C* **2011**, *115*, 19005−19011.
(50) Jiang, T.; Xu, K.; Ji, S. FTIR Studies on the Spectral Changes of the Surface Functional Groups of Ultradispersed Diamond Powder Synthesized by Explosive Detonation after Treatment in Hydrogen, Nitrogen, Methane and Air at Different Temperatures. *J. Chem. Soc., Faraday Trans.* **1996**, *92*, 3401.
(51) Mathkar, A.; Tozier, D.; Cox, P.; Ong, P.; Galande, C.; Balakrishnan, K.; Leela Mohana Reddy, A.; Ajayan, P. M. Controlled, Stepwise Reduction and Band Gap Manipulation of Graphene Oxide. *J. Phys. Chem. Lett.* **2012**, *3*, 986−991.
(52) Cheng, C. L.; Chen, C. F.; Shaio, W. C.; Tsai, D. S.; Chen, K. H. The CH Stretching Features on Diamonds of Different Origins. *Diamond Relat. Mater.* **2005**, *14*, 1455−1462.
(53) Krueger, A.; Liang, Y.; Jarre, G.; Stegk, J. Surface Functionalisation of Detonation Diamond Suitable for Biological Applications. *J. Mater. Chem.* **2006**, *16*, 2322.
(54) Joseph, J.; Jemmis, E. D. Red-, Blue-, or No-Shift in Hydrogen Bonds: A Unified Explanation. *J. Am. Chem. Soc.* **2007**, *129*, 4620−4632.
(55) Paul, J. B.; Provencal, R. A.; Chapo, C.; Roth, K.; Casaes, R.; Saykally, R. J. Infrared Cavity Ringdown Spectroscopy of the Water Cluster Bending Vibrations. *J. Phys. Chem. A* **1999**, *103*, 2972−2974.
(56) Ayers, G. P.; Pullin, A. D. E. The I.r. Spectra of Matrix Isolated Water species—I. Assignment of Bands to (H2O)2, (D2O)2 and HDO Dimer Species in Argon Matrices. *Spectrochim. Acta Part A Mol. Spectrosc.* **1976**, *32*, 1629−1639.
(57) Honegger, E.; Leutwyler, S. Intramolecular Vibrations of Small Water Clusters. *J. Chem. Phys.* **1988**, *88*, 2582−2595.
(58) Haldar, T.; Bagchi, S. Electrostatic Interactions Are Key to C═O N-Π* Shifts: An Experimental Proof. *J. Phys. Chem. Lett.* **2016**, *7*, 2270−2275.
(59) Gussoni, M.; Castiglioni, C. Infrared Intensities. Use of the CH-Stretching Band Intensity as a Tool for Evaluating the Acidity of Hydrogen Atoms in Hydrocarbons. *J. Mol. Struct.* **2000**, *521*, 1−18.
(60) Scheiner, S.; Kar, T. Spectroscopic and Structural Signature of the CH-O Hydrogen Bond. *J. Phys. Chem. A* **2008**, *112*, 11854−11860.

DOI: 10.1021/acs.jpcc.7b00721
J. Phys. Chem. C 2017, 121, 5185−5194

(61) Qian, W.; Krimm, S. Vibrational Spectroscopy of Hydrogen Bonding: Origin of the Different Behavior of the C−H···O Hydrogen Bond. *J. Phys. Chem. A* **2002**, *106*, 6628−6636.
(62) Asay, D. B.; Kim, S. H. Evolution of the Adsorbed Water Layer Structure on Silicon Oxide at Room Temperature. *J. Phys. Chem. B* **2005**, *109*, 16760−16763.
(63) Anderson, A.; Ashurst, W. R. Interfacial Water Structure on a Highly Hydroxylated Silica Film. *Langmuir* **2009**, *25*, 11549−11554.
(64) Torun, B.; Kunze, C.; Zhang, C.; Kühne, T. D.; Grundmeier, G. Study of Water Adsorption and Capillary Bridge Formation for SiO(2) Nanoparticle Layers by Means of a Combined in Situ FT-IR Reflection Spectroscopy and QCM-D Set-Up. *Phys. Chem. Chem. Phys.* **2014**, *16*, 7377−7384.
(65) Scatena, L. F.; Brown, M. G.; Richmond, G. L. Water at Hydrophobic Surfaces: Weak Hydrogen Bonding and Strong Orientation Effects. *Science* **2001**, *292*, 908−912.
(66) Walrafen, G. E.; Fisher, M. R.; Hokmabadi, M. S.; Yang, W.-H. Temperature Dependence of the Low- and High-Frequency Raman Scattering from Liquid Water. *J. Chem. Phys.* **1986**, *85*, 6970.
(67) Burikov, S. A.; Dolenko, T. A.; Velikotnyi, P. A.; Sugonyaev, A. V.; Fadeev, V. V. The Effect of Hydration of Ions of Inorganic Salts on the Shape of the Raman Stretching Band of Water. *Opt. Spectrosc.* **2005**, *98*, 235−239.
(68) Burikov, S. A.; Dolenko, T. A.; Fadeev, V. V.; Vlasov, I. I. Revelation of Ion Hydration in Raman Scattering Spectral Bands of Water. *Laser Phys.* **2007**, *17*, 1255−1261.
(69) Wernet, P.; Nordlund, D.; Bergmann, U.; Cavalleri, M.; Odelius, M.; Ogasawara, H.; Näslund, L. A.; Hirsch, T. K.; Ojamäe, L.; Glatzel, P.; et al. The Structure of the First Coordination Shell in Liquid Water. *Science* **2004**, *304*, 995−999.
(70) Chen, W.; Wu, X.; Car, R. X-Ray Absorption Signatures of the Molecular Environment in Water and Ice. *Phys. Rev. Lett.* **2010**, *105*, 17802.
(71) Juurinen, I.; Pylkkänen, T.; Sahle, C. J.; Simonelli, L.; Hämäläinen, K.; Huotari, S.; Hakala, M. Effect of the Hydrophobic Alcohol Chain Length on the Hydrogen-Bond Network of Water. *J. Phys. Chem. B* **2014**, *118*, 8750−8755.
(72) Huang, N.; Schlesinger, D.; Nordlund, D.; Huang, C.; Tyliszczak, T.; Weiss, T. M.; Acremann, Y.; Pettersson, L. G. M.; Nilsson, A. Microscopic Probing of the Size Dependence in Hydrophobic Solvation. *J. Chem. Phys.* **2012**, *136*, 074507.
(73) Velasco-Velez, J.-J.; Wu, C. H.; Pascal, T. A.; Wan, L. F.; Guo, J.; Prendergast, D.; Salmeron, M. The Structure of Interfacial Water on Gold Electrodes Studied by X-Ray Absorption Spectroscopy. *Science* **2014**, *346*, 831−834.
(74) Pylkkänen, T.; Giordano, V. M.; Chervin, J.-C.; Sakko, A.; Hakala, M.; Soininen, J. A.; Hämäläinen, K.; Monaco, G.; Huotari, S. Role of Non-Hydrogen-Bonded Molecules in the Oxygen K-Edge Spectrum of Ice. *J. Phys. Chem. B* **2010**, *114*, 3804−3808.
(75) Myneni, S.; Luo, Y.; Näslund, L. Å.; Cavalleri, M.; Ojamäe, L.; Ogasawara, H.; Pelmenschikov, A.; Wernet, P.; Väterlein, P.; Heske, C.; et al. Spectroscopic Probing of Local Hydrogen-Bonding Structures in Liquid Water. *J. Phys.: Condens. Matter* **2002**, *14*, L213−L219.
(76) Hammer, N. I.; Shin, J.-W.; Headrick, J. M.; Diken, E. G.; Roscioli, J. R.; Weddle, G. H.; Johnson, M. A. How Do Small Water Clusters Bind an Excess Electron? *Science* **2004**, *306*, 675−679.
(77) Herbert, J. M.; Head-Gordon, M. Charge Penetration and the Origin of Large O-H Vibrational Red-Shifts in Hydrated-Electron Clusters, (H2O)n-. *J. Am. Chem. Soc.* **2006**, *128*, 13932−13939.
(78) Roscioli, J. R.; Hammer, N. I.; Johnson, M. A. Infrared Spectroscopy of Water Cluster Anions, (H2O)n = 3−24-)in the HOH Bending Region: Persistence of the Double H-Bond Acceptor (AA) Water Molecule in the Excess Electron Binding Site of the Class I Isomers. *J. Phys. Chem. A* **2006**, *110*, 7517−7520.
(79) Maier, F.; Riedel, M.; Mantel, B.; Ristein, J.; Ley, L. Origin of Surface Conductivity in Diamond. *Phys. Rev. Lett.* **2000**, *85*, 3472−3475.
(80) Chen, W.; Qi, D.; Gao, X.; Wee, A. T. S. Surface Transfer Doping of Semiconductors. *Prog. Surf. Sci.* **2009**, *84*, 279−321.
(81) Marcon, L.; Riquet, F.; Vicogne, D.; Szunerits, S.; Bodart, J.-F.; Boukherroub, R. Cellular and in Vivo Toxicity of Functionalized Nanodiamond in Xenopus Embryos. *J. Mater. Chem.* **2010**, *20*, 8064.
(82) Zhu, D.; Zhang, L.; Ruther, R. E.; Hamers, R. J. Photo-Illuminated Diamond as a Solid-State Source of Solvated Electrons in Water for Nitrogen Reduction. *Nat. Mater.* **2013**, *12*, 836−841.
(83) Grall, R.; Girard, H.; Saad, L.; Petit, T.; Gesset, C.; Combis-Schlumberger, M.; Paget, V.; Delic, J.; Arnault, J.-C.; Chevillard, S. Impairing the Radioresistance of Cancer Cells by Hydrogenated Nanodiamonds. *Biomaterials* **2015**, *61*, 290−298.

DOI: 10.1021/acs.jpcc.7b00721
J. Phys. Chem. C 2017, 121, 5185−5194